Chemical and Process Engineering: New Frontiers, 2026, 47(1), e128
DOI: 10.24425/cpe.2026.158126

Adsorptive removal of Cr(III) ions from aqueous solutions using magnetic activated carbon

Jakub Mokrzycki[1*], Agnieszka Orzechowska-Zięba[1], Waldemar Tokarz[2], Katarzyna Berent[3], Eliza Wolak[1]

[1] AGH University of Krakow, Faculty of Energy and Fuels, Al. A. Mickiewicza 30, 30-059 Krakow, Poland
[2] AGH University of Krakow, Faculty of Physics and Applied Computer Science, Al. A. Mickiewicza 30, 30-059 Krakow, Poland
[3] AGH University of Krakow, Academic Centre for Materials and Nanotechnology, Al. A. Mickiewicza 30, 30-059 Krakow, Poland

Abstract
Water contamination with heavy metals, including chromium ions, poses a significant environmental and health threat because of their toxic, carcinogenic, and mutagenic properties. Although Cr(III) is an essential trace element, its potential oxidation to Cr(VI) necessitates effective removal strategies. Among various techniques, adsorption is considered the most cost-effective and efficient method for chromium removal. Activated carbons (ACs), owing to their high surface area and porosity, are widely used adsorbents. However, their recovery from aqueous systems is challenging. To address this, magnetic activated carbons were synthesized by impregnating ACs with iron oxide (Fe_3O_4) nanoparticles via co-precipitation, enabling easy separation using an external magnetic field. The modified activated carbons obtained were characterised by XRD, N_2 sorption at −196 °C, FT-IR, SEM-EDS, iodine adsorption number analysis, and magnetisation measurements. Their adsorption performance for the removal of Cr(III) ions was evaluated at an adsorbent dose of 1 $g \cdot L^{-1}$ and a solution pH of 5.00, using initial Cr(III) concentrations ranging from 30 to 400 $mg \cdot L^{-1}$, which fall within the moderate concentration range typical of industrial wastewater. The data were fitted to Langmuir and Freundlich isotherm models to elucidate the adsorption mechanisms. From the obtained results it was proved, that the introduction of iron nanoparticles onto the surface of the AC, did not cause a significant decrease in the adsorption properties. The adsorption capacity varied in the range from 22.37 to 25.84 mg Cr(III) g^{-1}. In addition, the effects of solution pH, adsorbent dose, adsorption temperature, and three successive adsorption cycles were investigated using single-point adsorption experiments.

Keywords
activated carbon, adsorption, Cr(III) removal, magnetic adsorbents

* **Corresponding author, e-mail:**
jmokrzycki@agh.edu.pl

Article info:
Received: 06 November 2025
Revised: 03 February 2026
Accepted: 11 February 2026

1. INTRODUCTION

Water pollution with heavy metals such as arsenic, chromium, mercury, and lead has become a major environmental concern (Briffa et al., 2020). The toxic impact on human health is reflected in their carcinogenic, mutagenic, and teratogenic effects. Chromium is classified as one of the most abundant heavy metals on Earth, having two stable forms in an aqueous environment: trivalent Cr(III) and hexavalent Cr(VI) (Irshad et al., 2023; Mokrzycki et al., 2021a). The most harmful form of chromium form i.e. Cr(VI), is being released into the water from electroplating, tanning, dyeing, and chromate synthesis industries. However, Cr(III) is an important microelement, nearly 300-fold less toxic than its hexavalent counterpart. However, there is a risk of Cr(III) oxidation to Cr(VI), so the overall chromium content in the environment must be strictly monitored. The concentration of Cr(III) ions present in tannery facilities can reach values of approximately 3000 $mg \cdot L^{-1}$, although even higher concentrations up to 10,000 $mg \cdot L^{-1}$ have been reported (Bonola et al., 2022). Other sources indicate that the concentration in wastewater can be around 100 $mg \cdot L^{-1}$ (Dias et al., 2018). Considering legal regulations related to drinking water safety, these concentrations must be significantly reduced to levels of approximately 0.05 $mg \cdot L^{-1}$ (WHO) or 0.1–0.5 $mg \cdot L^{-1}$, according to the China's Emission Standards of Pollutants for the Inorganic Chemical Industry (GB 31573-2015) (Yuan et al., 2025). As for the European Union countries, including Poland, the permissible level of chromium complies with the WHO standard of 0.05 $mg \cdot L^{-1}$, with a target value of 0.025 $mg \cdot L^{-1}$ to be achieved by 12 January 2036 (Rusiniak et al., 2024). The most common methods of chromium removal involve electrodialysis, membrane technologies, coagulation, and adsorption. Among them, adsorption is considered the cheapest and most efficient (Flieger et al., 2020; Li et al., 2023).

Commonly used chromium ion adsorbents involve: biochars (Michalak et al., 2019; Mokrzycki et al., 2021a; 2021b), zeolites (Dimas Rivera et al., 2021; Liu et al., 2022), magnetic Fe_3O_4 at alkali treated coal fly ash (Zhang and Yu, 2018) and activated carbons (ACs) (Gęca et al., 2022). Synthetic materials like metal-organic framework (HKUST-1), have been also reported to possess adsorption properties towards removal of chromium ions from aqueous solutions (Irshad et al., 2023; Mokrzycki et al., 2024; Shahrokhi-Shahraki et al., 2021).

Activated carbon due to its high porosity, high surface area, and chemical stability, has become one of the most efficient adsorbents of both organic and inorganic pollutants from aqueous environment (Mokrzycki et al., 2020). Using activated carbon (AC) brings the problem of difficult separation and recovery. To overcome this problem, magnetic separation technology can be safe and effective, time-saving and cheap. The combination of magnetic materials and active carbons not only preserves the original chemical and physical properties of AC's, but also possesses the characteristics of magnetic separation (Nata et al., 2024; Wijaya et al., 2024).

To improve adsorption properties and ease isolation from the aquatic environment, magnetic iron nanoparticles can be introduced into carbonaceous material surface (Ahmad et al., 2020).

The magnetic carbons permit the easy separation of the saturated adsorbent after the adsorption process by an external magnetic field, which implies less waste of adsorbent materials in comparison with conventional separation approaches, like centrifugation and filtration (Wu et al., 2023).

Laurent et al. (2010) have listed different methods to produce magnetic particles, including: co-precipitation, sol–gel or electrospray synthesis, and sonochemical, hydrothermal or solvothermal reactions. However, the most popular approach to obtain magnetic nanoparticles is the co-precipitation of iron salts (Mao et al., 2022). In the co-precipitation method, Fe_3O_4 nanoparticles are formed from an aqueous solution containing Fe(II) and Fe(III) salts in the stoichiometric ratio. Fe_3O_4 particles precipitate by adding basic reagents, such as NaOH and NH_4OH, to get a pH in 8–14 range (Krishna Kumar et al., 2022).

Maneechakr and Mongkollertlop (2020) have obtained 19.92 $mg \cdot g^{-1}$ adsorption capacity of Cr(III) ions for magnetic biochar doped with $KMnO_4$. Such adsorbent was also effective towards removal of other heavy metal ions including: Pb(II), Cd(II), and Hg(II).

In research of Azam et al. (2021), low-cost adsorbents were investigated, including raw date pits and chemically treated date pits, aiming to apply these materials to investigate the adsorption behavior of Cr(III) and Cd(II) ions from wastewater. The optimum pH for achieving maximum adsorption capacity was found to be approximately 7.8. The obtained adsorption capacities for Cr(III) at 20 °C were 400 $mg \cdot g^{-1}$ (treated majdool date pits adsorbent) and 388 $mg \cdot g^{-1}$ (treated sagai date pits adsorbent), respectively. It should be however noted, that at such a pH value, some precipitation of the chromium(III) hydroxide might also occur, hence changing the mechanism of Cr(III) removal from adsorption onto adsorbent into precipitation (Guan et al., 2022).

Magnetic activated carbons have attracted increasing attention due to their facile separation from aqueous media through the application of an external magnetic field. Desorption of adsorbed Cr(III) and Cr(VI) ions can be achieved using eluents such as NaOH (1–2 M), NH4OH, or HCl, which have been reported to be effective for adsorbent regeneration. Using these reagents, chromium recovery efficiencies of up to approximately 56% have been reported, with 2 M NaOH showing the highest performance (Ahmad et al., 2020). Other studies focus on the application of low concentrated 0.1M HNO_3 which was reported to recover up to 80% of chromium ions without causing damage to the adsorption sites, allowing reuse of the adsorbent (Abenojar et al., 2024). However, it should be held in mind, that the risk of re-emissions of iron from the magnetic activated carbons to the solutions remains a potential limitation of these materials. In the work of Sangkarak et al. (2024), it was proved that low concentrations of NaOH (0.01–0.1 M) used for regeneration of magnetic adsorbents, did not cause a notable drop in the adsorption and magnetic properties even in a five-cycle experiment, with a 50% Cr(III) removal efficiency.

The main goal of this research was to synthesize a series of magnetic activated carbons via a simple impregnation method and iron nanoparticle (Fe_3O_4) precipitation onto the activated carbon's surface. Obtained magnetic activated carbons were investigated by means of XRD, N_2 sorption at −196 °C, FT-IR, iodine adsorption number, and magnetization. The investigated materials were subsequently employed as adsorbents for the removal of Cr(III) ions from aqueous solutions with moderate Cr(III) concentrations ranging from 30 to 400 $mg \cdot L^{-1}$, relative to those typically found in industrial wastewaters. The adsorbents were characterized by an enhanced ease of separation from the aqueous system. The experimental results of Cr(III) removal were correlated with the Langmuir and Freundlich isotherm models to gain a better understanding of the potential mechanisms, that guided the adsorption process. The effect of solution pH, adsorbent dose, and adsorption temperature was investigated in single-point experiments. Despite numerous works regarding adsorption using magnetic carbonaceous materials, only few considered removal of Cr(III) ions, showing a knowledge gap in this field.

2. MATERIALS AND METHODS

2.1. Material preparation

Pristine activated carbon (CWZ) was modified by incorporation of iron nanoparticles (NPs) into its surface. The synthesis procedure was based on the modified method demonstrated in the work of Alagarsamy and Jiang (2017). Briefly, in a two separate beakers, 2.13g of $FeCl_3$ (Avantor Performance Materials Poland, Gliwice, Poland) and 0.80g of $FeCl_2 \cdot 4H_2O$ (Avantor Performance Materials Poland, Gliwice, Poland) was dissolved in 200 mL (Solution A) and 100 mL (Solution B) of deionized water. In a separate beaker, 2g of activated CWZ was weighed. Next, 1 dose of the solutions was added, which consisted of 8 mL of Solution A and 4 mL of Solution B. The resultant solution with AC was mixed using a magnetic stirrer

for 10 min in an oil bath at 40 °C. To the resultant mixture, 1 mL of 8M NH_4OH solution (Avantor Performance Materials Poland, Gliwice, Poland) was added dropwise and mixed for another 10 min. The mixture was then filtered and washed with deionized water several times. The obtained material was air dried overnight followed by drying in an oven at 110 °C for 24h. Three different doses of the solutions were used for material preparation: 1 (8 mL of Solution A+4 mL of Solution B+1 mL of NH_4OH), 5 (40 mL of Solution A+20 mL of Solution B1+5 mL of NH_4OH), or 10 (80 mL of Solution A+40 mL of Solution B+10 mL of NH_4OH) per 2g of AC, and denoted as: 1P, 5P, and 10P, respectively.

2.2. Material characterization

2.2.1. X-ray diffraction (XRD)

X-ray diffraction patterns were collected using PANalytical Empyrean diffractometer (Malvern Panalytical, Malvern, UK). The radiation source was CuK$\alpha\lambda$ = 1.5406 Å. The diffractograms were collected in the 2θ range from 10 to 70°, with a 0.013° step.

2.2.2. Fourier-Transform Infrared Spectroscopy (FT-IR)

Fourier-Transform Infrared spectra were collected using spectrometer (Nicolet 6700, Thermoscientific, Madison, WI, USA). Each sample was mixed with KBr, prior to the measurement with a ratio of 1:100. Wavenumbers were collected in a range from 4000 to 400 cm^{-1}.

2.2.3. N_2 sorption at –196 °C

The textural properties of the investigated activated carbons were evaluated by means of Micromeritics 3Flex Surface Characterization gas adsorption analyzer (Micromeritics, Norcross, GA, USA). Prior to the analysis, samples were degassed at 150 °C for 12h under vacuum. The specific surface area (S_{BET}) was calculated according to the Brunauer–Emmet–Teller model. The micropore volume (V_{mic}) was calculated using the Horvath-Kawazoe method (*H-K*).

2.2.4. SEM-EDS

The surface morphology and iron coating of activated carbon were characterized using scanning electron microscopy (SEM) combined with energy-dispersive X-ray spectroscopy (EDS). SEM observations were carried out using secondary electron (SE) and backscattered electron (BSE) detectors to evaluate, respectively, the surface morphology and the degree and uniformity of iron coverage through atomic number contrast. Elemental composition and the spatial distribution of iron on the material surface were determined by EDS analysis. All measurements were performed using an FEI Versa 3D scanning electron microscope equipped with an Oxford Instruments Ultim Max EDS spectrometer, operating at an accelerating voltage of 12 kV.

2.2.5. Iodine adsorption number (LI)

Iodine adsorption number (*LI*) was evaluated by means of Standard Test Method [4]ASTM D4607-14 (2021). The amount of iodine adsorbed (in mg) by 1g of carbon is called the iodine number. This method is used to assess the quality of carbons intended for adsorption from solutions of dissolved substances with dimensions similar to the size of iodine molecules – diameter of about 1 nm. Briefly, 0.2 g of the examined AC was mixed with 5% HCl (Avantor, Gliwice, Poland) and 0.1 M solution of iodine. Next, the prepared solution was titrated with 0.1 M sodium thiosulfate (Avantor, Gliwice, Poland) using starch as an indicator.

2.2.6. Magnetization

The magnetization dependence as a function of the external magnetic field was measured on a LakeShore model 7300 (VMS, Lakeshore Instruments, USA) vibrating sample magnetometer at room temperature.

2.3. Trivalent chromium adsorption statics

Removal of Cr(III) ions from aqueous solutions was performed to investigate the adsorption statistics. The obtained results were correlated with adsorption isotherm models: Langmuir and Freundlich, given in their linear forms in Equation (1) and Equation (2), respectively.

$$\frac{q_{eq}}{C_{eq}} = \frac{C_{eq}}{q_{max}} + \frac{1}{K_L \cdot q_{max}} \tag{1}$$

$$\ln(q_{eq}) = \ln(K_F) + \frac{1}{n}\ln(C_{eq}) \tag{2}$$

where, q_{eq} [$mg \cdot g^{-1}$] – is the adsorption capacity et equilibrium; C_{eq} [$mg \cdot L^{-1}$] – is the concentration of Cr(III) ions at equilibrium; q_{max} [$mg \cdot g^{-1}$] – is the monolayer adsorption capacity of the adsorbent; K_L [$L \cdot mg^{-1}$] – is the Langmuir model constant; K_F [$mg^{1-1/n}L^{1/n}g^{-1}$] – is the Freundlich model constant; $1/n$ – is the heterogeneity factor.

Based on the Langmuir model a dimensionless parameter R_L was calculated according to the Equation (3).

$$R_L = \frac{1}{1 + C_0 \cdot K_L} \tag{3}$$

where, K_L [$L \cdot mg^{-1}$] – is the Langmuir model constant; and C_0 [$mg \cdot L^{-1}$] – is the initial concentration of Cr(III) ions in the solution (selected concentrations were 30 and 400 mg Cr(III) $\cdot L^{-1}$, respectively). The values obtained from the R_L

parameter calculation reflect the nature of the adsorption process, where $R_L > 1$ – unfavorable adsorption, $R_L = 1$ – linear adsorption, $R_L = 0$ – irreversible adsorption, and $1 < R_L < 0$ – favorable adsorption (Mokrzycki et al., 2021b).

Adsorption experiments were performed according to the following procedure. In a 50 mL flasks, 40 mg of magnetic carbons was weighed. Freshly prepared solutions of $Cr(NO_3)_3 \cdot 9H_2O$ (Honeywell-Fluka, Bucharest, Romania) with initial concentrations of: 30, 60, 90, 120, 150, 200, 300, 400 mg Cr(III) g^{-1} and pH adjusted to 5.00 using 0.1M solutions of KOH or HNO_3 (Avantor Performance Materials Poland S.A., Gliwice, Poland) were poured (40 mL) into the flasks and mixed using a VS15O laboratory shaker (LAUDA DR. R. WOBSER GMBH & CO. KG, Lauda-Königshofen, Germany) at 180 rpm for 2 h. Next, the solutions were filtrated and 4 mL of solution was collected and mixed with 0.095 g of disodium versenate dihydrate (Avantor Performance Materials Poland S.A., Gliwice, Poland) and placed in a water bath at $80 \pm 2\,^{\circ}C$ for 10 min. After rapid cooling, samples were analyzed using a spectrophotometer UV-5600 (Shanghai Matash Instruments, Shanghai, China) at a wavelength of 540 nm. As a blank sample 4 mL of deionized water was mixed with 0.095g of disodium versenate dihydrate and analyzed according to the abovementioned procedure. All the measurements were performed in duplicate.

The effects of solution pH (3, 5, and 6), adsorbent dose (0.5, 1, and 2 $g \cdot L^{-1}$), adsorption temperature (20, 30, and 40 °C), and adsorption over three successive cycles were investigated to better understand their influence on process efficiency using single-point adsorption measurements. In all experiments, aqueous solutions containing 100 $mg \cdot L^{-1}$ of Cr(III) ions were prepared. The contact time was fixed at 2 h, during which the samples were vigorously mixed.

For studies on the effects of adsorption temperature and adsorption cycles, the adsorbent dose was maintained at 1 $g \cdot L^{-1}$ and the solution pH was adjusted to 5.00. An adsorbent dose of 1 $g \cdot L^{-1}$ was also used in the experiments examining the effect of solution pH, whereas a solution pH of 5.00 was employed for experiments assessing the effect of adsorbent dose.

Adsorption cycle experiments were conducted by recovering the adsorbent after each adsorption step, rinsing it with water, and drying it at 110 °C overnight prior to reuse in the subsequent cycle. All the measurements were performed in duplicate.

3. RESULTS AND DISCUSSION

The phase composition of the investigated materials is summarized in Fig. 1. The presented XRD pattern of CWZ activated carbon clearly indicates the amorphous character of the material. Two characteristic broad peaks with their maximum located at 2θ: 24.0, and 42.6° were assigned to the (002), and (100) planes, respectively (Wang et al., 2020b). The Fe_3O_4 nanoparticle planes were identified at 2θ: 30.4° (220), 35.7° (311), 43.3° (400), 53.8° (422), 57.3° (511), and 63.1° (440), according to JCPDS card no. 85-1436 (Silva et al., 2013). With an increase in the dose of solution used for magnetic activated carbon preparation, the intensity of characteristic peaks of AC diminished, while for Fe_3O_4 NPs slightly increased and were the most visible for sample 10P. A similar observation was reported by Do et al. (2011).

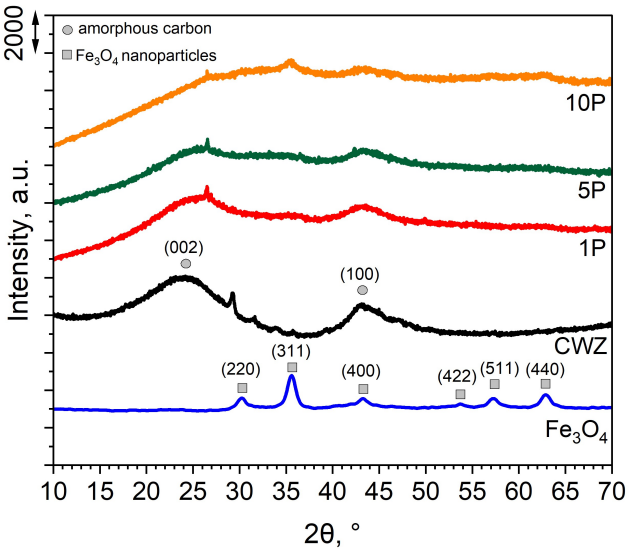

Figure 1. XRD pattern of investigated samples.

The adsorption capacity and adsorption characteristics of activated carbon are not only related to the size of the specific surface area but also related to its pore structure and distribution.

The specific surface area of the 1P sample was the highest among the investigated series (1221 $m^2 \cdot g^{-1}$). A similar observation was evidenced by Song et al. (2019), where the specific surface area of the magnetic activated carbon increased after introduction of nano-Fe_3O_4. This phenomenon was explained by incorporation of small iron nanoparticles within the pores. Hence, iron impregnation resulted in pore shrinkage without causing pore blockage. In fact, according to research by the authors' earlier work (Buczek and Wolak, 2008), it was found that the activated carbon CWZ was microporous and had slit-shaped or bottle-shaped pores. The pores in activated carbon greatly affect the physical adsorption process. The presence of iron nanoparticles on the AC surface affected the structure and properties of the activated carbon surface, which in turn affected their adsorption of toxic metals from water (Gęca et al., 2022). After modification of the activated carbons with iron nanoparticles, partial blockage of the porous structure of activated carbon occurred, resulting in a decrease in the specific surface area of the adsorbent and a smaller micropores volume (Table 1). The iodine adsorption number also indicates a decrease in the amount of adsorbed iodine with an increase in the amount of introduced iron nanoparticles. The diameter of the sorbed iodine molecule is much larger than the nitrogen

molecule, hence also for sample 1P a decrease in the iodine number was observed compared to the initial CWZ sample.

To assess the quality of the obtained adsorbents, the specific surface area (S_{BET}), micropore volume (V_{mic}) and iodine adsorption number (LI) were determined. The results are presented in Table 1, while the N_2 adsorption-desorption isotherms are presented in Fig. 2.

Table 1. The surface properties of adsorbent

Sample	S_{BET} [$m^2 \cdot g^{-1}$]	V_{mic} [$cm^3 \cdot g^{-1}$]	LI [$mg \cdot g^{-1}$]
CWZ	1006	0.413	921
1P	1221	0.501	800
5P	924	0.380	610
10P	598	0.249	480

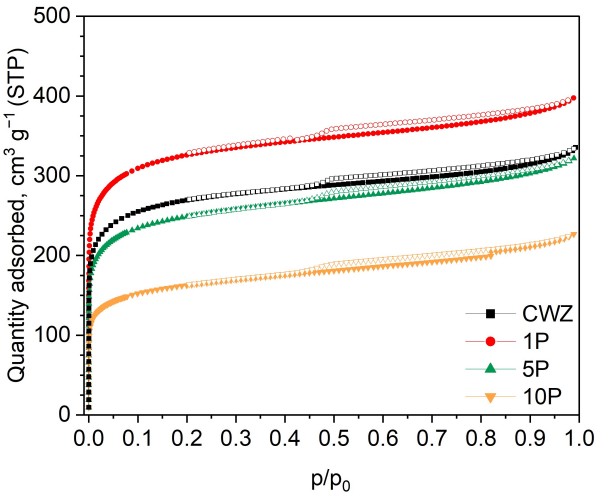

Figure 2. N_2 adsorption-desorption isotherms at −196 °C over investigated materials. Solid symbol refers to adsorption, while empty inside symbol refers to desorption stage.

The adsorption isotherm shapes were identified as type IA according to the IUPAC classification, indicating a microporous character of the material surfaces. Moreover, the materials are characterized by narrow micropores (< 1 nm). The hysteresis observed during the desorption stage was identified as type H4, which often accompanies type IA isotherms for materials in which mesopores are also present. (Thommes et al., 2015).

The FT-IR spectra are presented in Fig. 3. The spectra recorded for pristine CWZ activated carbon and iron nanoparticles modified carbons exhibited O-H vibrations at about 3375 cm^{-1} implying presence of moisture, along with vibration at about 1640 cm^{-1}. A peak at 668 cm^{-1} was present for 1P, 5P, and 10P samples and its intensity increased along with higher concentration of nanoparticles dose, indicating presence of Fe_3O_4 nanoparticles over the material's surface.

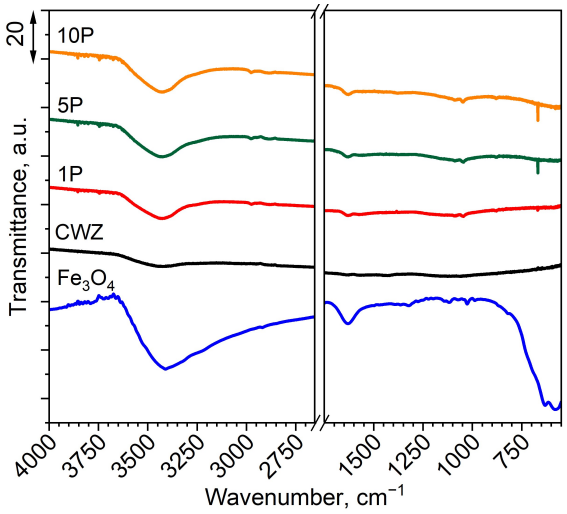

Figure 3. FT-IR spectra of investigated samples.

The magnetization curves of the evaluated samples are presented in Fig. 4. The sample marked as P1 measured as a function of the external magnetic field intensity has a typical course for diamagnetic materials. As the field increases, magnetic moments are induced inside the material with the opposite direction to the external field (Cullity and Graham, 1974). In large fields, saturation occurs at the level of 0.04 emu $\cdot g^{-1}$. The situation changes for the CWZ sample signal, where the combination of diamagnetism and paramagnetism can be observed. Here, in addition to the induced moment opposing the external magnetic field, there are particles with their own permanent magnetic moments, which reorient in accordance with the external magnetic field. The slope of the magnetization curve in fields up to 2 kOe suggests a superparamagnet or soft ferromagnet. In the case of the P5 sample, we have a magnetization course that is probably the result of the overlap of magnetization from two phases: one superparamagnetic or soft ferromagnetic to the paramagnetic or antiferromagnetic phase of the latter. The magnetization in the CWZ, P1, P5 and P10 samples systematically increases, which indicates presence of particles with a magnetic moment. Also when placed in the solution and introduced to the magnetic field, it can be clearly seen that after just 2 min of exposure the material was rapidly aggregated at the corner of the beaker, implying the opportunity to recover the magnetic AC from the solution (Figure 5).

SEM images of the investigated materials are summarized in Fig. 6. As shown, the materials exhibit morphology typical of activated carbons, with numerous pores and cavities visible on the material surfaces (Figs. 6a_1–6d_2). The corresponding EDS mappings of the main elements constituting the activated carbons – carbon, oxygen, and iron (for the modified materials) – are presented in Figs. 6a_3–6d_5. For materials containing introduced iron nanoparticles, an increase in the surface iron content is observed with increasing dose of the solution used during material preparation. For the 5P and 10P samples, some segregation of iron species can be observed; although iron remains relatively evenly distributed across the activated carbon surface.

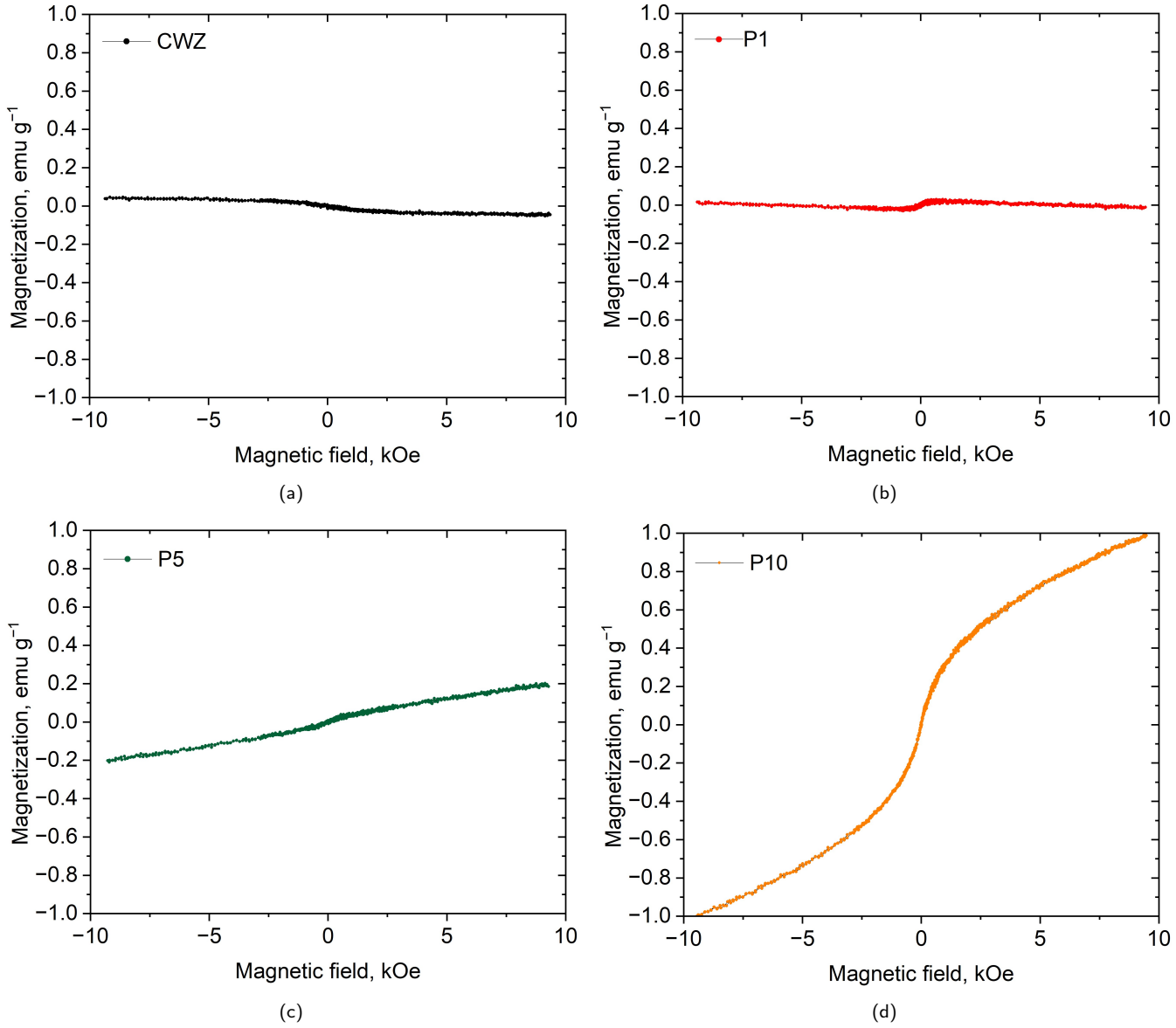

Figure 4. Magnetization curves of investigated samples.

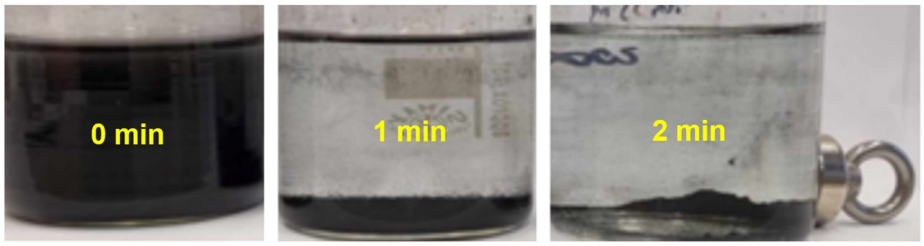

Figure 5. The effect of magnetic field on the magnetic activated carbon (10P).

The chemical composition of the investigated materials was examined using EDS mapping, and the results are summarized in Table 2. For materials modified by the introduction of iron nanoparticles, the Fe content (at.%) increased with increasing dose of the solution used during material preparation, from 0.23 (1P) to approximately 3.90 at.% (10P).

Adsorption isotherms allowed to evaluate the AC's effectiveness towards removal of Cr(III) ions from aqueous phase. The experimental data were correlated with the Langmuir and Freundlich isotherm models as presented in Fig. 7. The adsorption model parameters are summarized in Table 3. Based on the regression coefficient values, the Langmuir model was

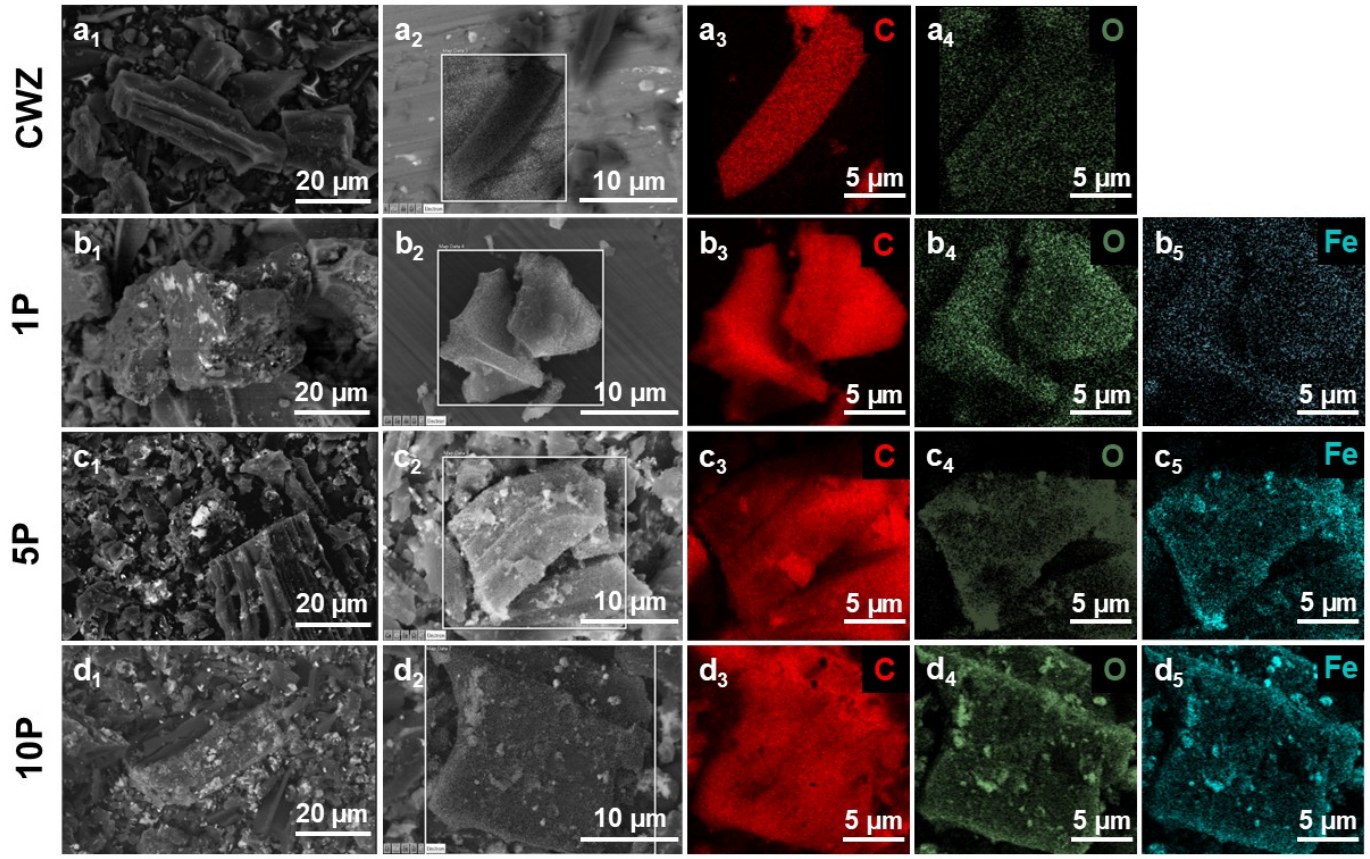

Figure 6. SEM images of investigated samples: CWZ (a), 1P (b), 5P (c), and 10P (d), where 1 – sample magnification of 5,000×, 2 – sample magnification of 12,000×, 3 – carbon EDS map, 4 – oxygen EDS map, 5 – iron EDS map.

Table 2. EDS chemical composition of investigated materials.

Sample	EDS chemical composition		
	C [at.%]	O [at.%]	Fe [at.%]
CWZ	98.46 ± 0.06	1.54 ± 0.06	–
1P	97.37 ± 0.25	2.40 ± 0.15	0.23 ± 0.06
5P	90.52 ± 1.86	7.99 ± 0.50	1.49 ± 0.19
10P	84.67 ± 0.49	11.43 ± 0.23	3.90 ± 0.26

found to be more suitable for description of the adsorption process of Cr(III) (Dada et al., 2012). According to models' assumptions, when the Langmuir adsorption model correlates with the experimental results, it indicates a monolayer adsorption of adsorbate over a uniform adsorbent surface. No interaction between the adsorbed molecules is being presumed. On the other hand, in correlation of the experimental results with Freundlich isotherm model a multilayer adsorption is being assumed, where the K_F model constant indicates the maximum adsorption capacity over the surface, whereas the $1/n$ constant reflects the affinity of adsorbate to the adsorbent and weather the adsorption is favorable ($1/n < 1$) or unfavorable ($1/n > 1$). From the obtained results it can be seen that $1/n$ value varied in the range from 0.076 to 0.246,

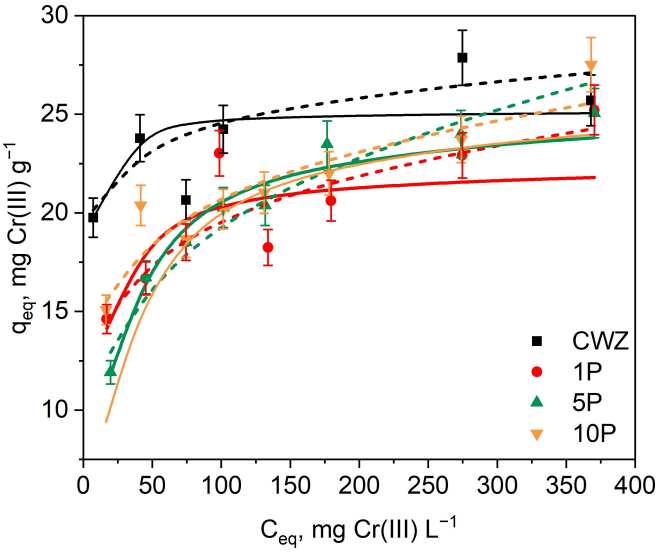

Figure 7. Adsorption isotherms at 20 °C of Cr(III) ions over investigated activated carbons – solid line (Langmuir model correlation), dashed line (Freundlich model correlation).

which implies favorable adsorption over the evaluated adsorbents. However, in the work of Mawlood et al. (2024), in the case of Cr(III) ion adsorption over the described activated

Table 3. Parameters of adsorption isotherm models.

Sample	Adsorption isotherm model							
	Langmuir					Freundlich		
	q_{max} [mg · g^{-1}]	K_L [L · mg^{-1}]	R_L (C_0 = 30 mg · L^{-1})	R_L (C_0 = 400 mg · L^{-1})	R^2	K_F [mg$^{1-1/n}$L$^{1/n}$g^{-1}]	$1/n$	R^2
CWZ	25.19	0.503	0.062	0.005	0.977	17.347	0.076	0.891
1P	22.37	0.101	0.248	0.024	0.732	9.146	0.165	0.808
5P	25.25	0.045	0.425	0.053	0.982	6.210	0.246	0.950
10P	25.84	0.035	0.488	0.067	0.989	9.876	0.161	0.868

carbons, the value of $1/n$ was > 1, which implied a strong adsorption affinity of Cr(III) ions to the adsorbent. The adsorption capacity as obtained from the Langmuir model was relatively high (39 mg · g^{-1}). At the same time, the adsorbent dose was significantly higher, than in the present study (1 g · L^{-1}) and varied from 16 to 48 g · L^{-1}. Also from the calculated R_L parameter obtained for low (30 mg · L^{-1}) and high (400 mg · L^{-1}) initial Cr(III) ion concentration in the solution, it can be clearly stated that R_L value in the range from 0.005 to 0.067 for lower initial concentrations and from 0.062 to 0.488 for higher initial concentrations, implies favorable adsorption process over the adsorbent surface, as was also indicated in the work of Rouibah et al. (2024).

To gain a better understanding of the various parameters that influence the adsorption of Cr(III) ions from aqueous solutions using the investigated activated carbons, the effect of adsorption temperature, solution pH, and adsorbent doses was investigated in a single-point adsorption tests. The obtained results are presented in Fig. 8. In Fig. 8a the summary

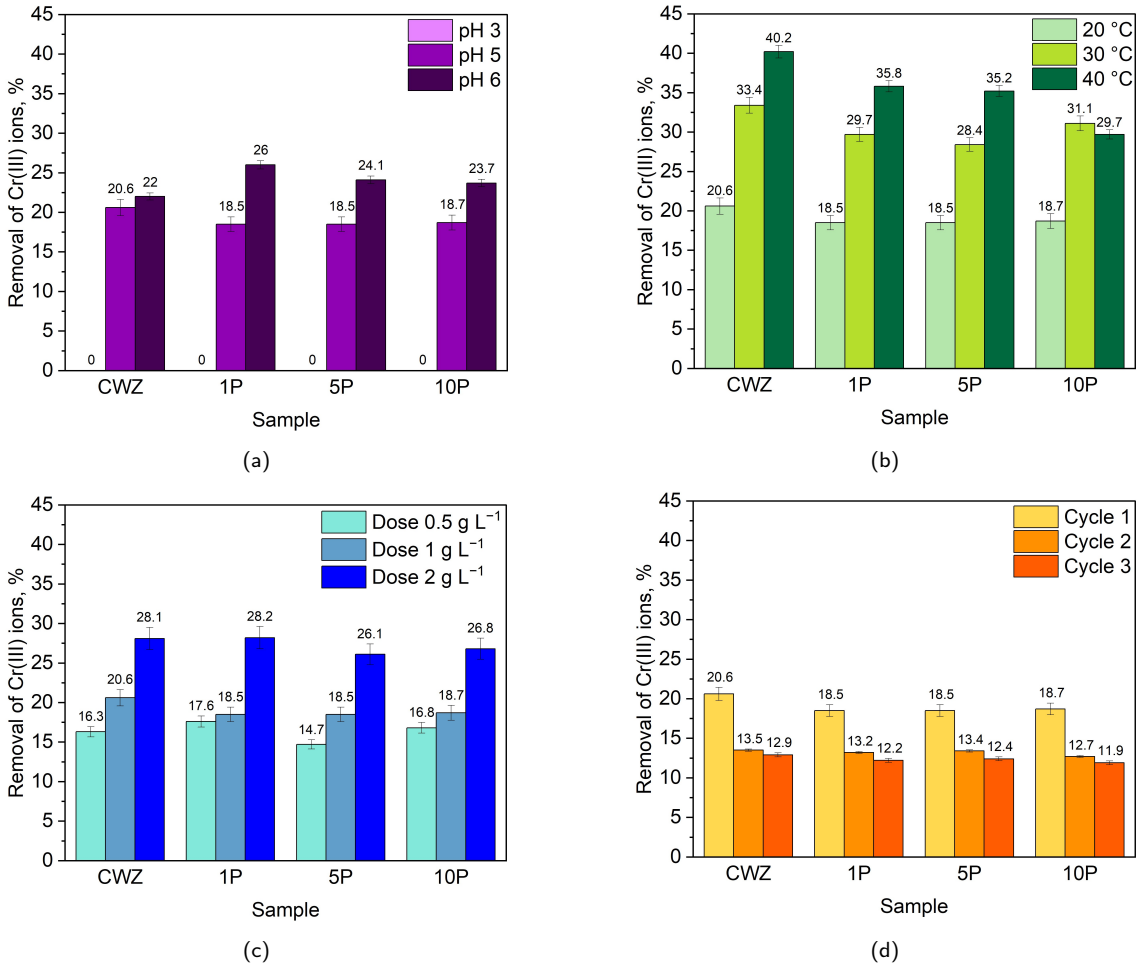

Figure 8. The effect of variables on the removal of Cr(III) ions: solution pH (3); adsorbent dose (b); adsorption temperature (c); and cycles of adsorption (d). Initial Cr(III) ions concentration: 100 mg · L^{-1}, contact time: 2 h.

of the effect of solution pH was compared. It can be seen that pH 3 completely blocked the adsorption over the investigated materials, probably due to the competition between Cr(III) ions and H_3O^+ ions in the solution, which occupied the adsorption active centers (Solis-Ceballos et al., 2023). An increase in the solution pH to 6, caused partial precipitation of Cr(III) ions and shift in the ions dominant form in the solution from Cr^{3+} (pH 3) and $CrOH^{2+}$ (pH 5) to $Cr(OH)_2^+$ (pH 6) (Xu et al., 2025). Increase in the adsorbent dose (Fig. 8b) caused nearly 2-fold increase in the removal of Cr(III) ions when doses of 0.5 and 2 $g \cdot L^{-1}$ were compared. From the experimental adsorption at various temperatures (Fig. 8c), it can be concluded that adsorption of Cr(III) ions is favored when the temperature increases, implying a endothermic character of the process, which was also confirmed for adsorption of Cr(III) ions on graphene oxide (Yang et al., 2014). Adsorption cycles were used to investigate the opportunity to reuse the materials (Fig. 8d). After the first cycle, the adsorption capacity dropped by about 30 percentage points for all the samples. Further reuse of the materials in 3rd cycle caused only a slight drop in the adsorption capacity, suggesting that there were still some unoccupied adsorption sites after the first and second adsorption cycles.

Table 4 presents a comparison of the adsorption parameters of Cr(III) ions from aqueous solutions and the sorption capacities of various sorbents, which are compared with the results obtained in the present study.

Table 4. Comparison of adsorption parameters using various adsorbents.

Adsorbent	Adsorption parameters	Adsorption capacity	Reference
Nanocomposite CaO/Fe_3O_4/SDS (sodium dodecyl sulfate)	Initial Cr(III) ions concentration: 5 $mg \cdot L^{-1}$ Temperature: 25 °C Adsorbent dose: 2 $g \cdot L^{-1}$ Adsorption pH: 5.0	6.40 $mg \cdot g^{-1}$	Tamjidi and Esmaeili (2019)
Magnetic biochar (MnO_2-modified biochar derived from palm kernel cake residue)	Initial Cr(III) ions concentration: 100 $mg \cdot L^{-1}$ Temperature: 30 °C Adsorbent dose: 8 $g \cdot L^{-1}$ Adsorption pH:-	19.92 $mg \cdot g^{-1}$	Maneechakr and Mongkollertlop (2020)
$NiFe_2O_4$/GO nanocomposite (graphene-oxide-decorated nickel ferrite)	Initial Cr(III) ions concentration: 100 $mg \cdot L^{-1}$ Temperature: 25 °C Adsorbent dose: 0.5 $g \cdot L^{-1}$ Adsorption pH: 6.5	17.00 $mg \cdot g^{-1}$	Ortiz-Quiñonez et al. (2023)
Nano-adsorbent $MnFe_2O_4$	Initial Cr(III) ions concentration: 1.5–186 $mg \cdot L^{-1}$ Temperature: 25 °C Adsorbent dose: 2 $g \cdot L^{-1}$ Adsorption pH: 5.0	39.60 $mg \cdot g^{-1}$	Eyvazi et al. (2020)
Fe_3O_4@SiO_2/Cs-DTPA (diethylenetriaminepentaacetic acid (DTPA)-chitosan functionalized magnetic silica)	Initial Cr(III) ions concentration: 2.5–30 $mg \cdot L^{-1}$ Temperature: 25 °C Adsorbent dose: 0.4 $g \cdot L^{-1}$ Adsorption pH: 4.0	22.24 $mg \cdot g^{-1}$	Wang et al. (2020a)
Biochar from coniferous wood	Initial Cr(III) ions concentration: 260–650 $mg \cdot L^{-1}$ Temperature: not defined Adsorbent dose: 50–150 $g \cdot L^{-1}$ Adsorption pH: not defined	32.00 $mg \cdot g^{-1}$	Frolova and Kharytonov (2019)
Camel dung-derived biochar	Initial Cr(III) ions concentration: 5–50 $mg \cdot L^{-1}$ Temperature: 22 °C Adsorbent dose: 2 $g \cdot L^{-1}$ Adsorption pH: 8.0	23.36 $mg \cdot g^{-1}$	Wilson et al. (2024)
Sodium bentonite, (Colombian bentonite)	Initial Cr(III) ions concentration: 50 $mg \cdot L^{-1}$ Temperature: 25 °C Adsorbent dose: 0.96 $g \cdot L^{-1}$ Adsorption pH: 3.5	6.44 $mg \cdot g^{-1}$	Castro- et al., (2020)

Table 4 continued on the next page

Table 4 continued from the previous page

Adsorbent	Adsorption parameters	Adsorption capacity	Reference
Natural metal – oxide material, derived from the enrichment of the quartz coastal sand	Initial Cr(III) ions concentration: 20 mg · L^{-1} Temperature: not specified Adsorbent dose: 5 g · L^{-1} Adsorption pH: 6-9	10.00 mg · g^{-1}	Shehu et al. (2023)
Magnetic Fe_3O_4@alkali-treated coal fly ash	Initial Cr(III) ions concentration: 100 mg · L^{-1} Temperature: 25 °C Adsorbent dose: 2 g · L^{-1} Adsorption pH: 4	212.31 mg · g^{-1}	Zhang and Yu (2018)
1P 5P 10P	Initial Cr(III) ions concentration: 30-400 mg · L^{-1} Temperature: 25 °C Adsorbent dose: 1 g · L^{-1} Adsorption pH: 5.0	22.37 mg · g^{-1} 25.25 mg · g^{-1} 25.84 mg · g^{-1}	This study

4. CONCLUSIONS

From the obtained results it can be clearly seen that regardless of the used adsorbent, the maximum adsorption capacity (q_{max}) was comparable and varied from 22.37 to 25.84 mg Cr(III) g^{-1}. Hence, the modification of the AC with iron nanoparticles did not cause any changes to the adsorption capacity towards removal of Cr(III) ions from aqueous phase. Moreover, the ability to separate the adsorbent from the solution was significantly improved even at a low dosage of introduced iron nanoparticles. It can be concluded that a simple precipitation method allows to introduce magnetic iron nanoparticles into the adsorbent surface and favors its removal from the solution, without any drop in the adsorption properties towards Cr(III) ions.

ACKNOWLEDGEMENTS

This study was funded for subvention of AGH University of Krakow, Faculty Energy and Fuels (project No. 16.16.210.476). Waldemar Tokarz acknowledges the support from the "Excellence Initiative-Research University" program for AGH University of Krakow.

SYMBOLS

C_0	initial concentration, mg · L^{-1}
C_{eq}	equilibrium concentration, mg · L^{-1}
K_F	Freundlich model constant, mg$^{1-1/n}$L$^{1/n}$g^{-1}
K_L	Langmuir model constant, L · mg^{-1}
LI	iodine adsorption number, m^2 g^{-1}
q_{eq}	adsorption capacity at equilibrium, mg · g^{-1}
q_{max}	monolayer adsorption capacity, mg · g^{-1}
R_L	dimensionless parameter from Langmuir model
S_{BET}	specific surface area as obtained from Brunauer–Emmet–Teller isotherm, m^2 g^{-1}
V_{mic}	volume of micropores, cm^3 g^{-1}
$1/n$	heterogeneity factor

Abbreviations

AC	activated carbon
BSE	backscattered electron detector
FT-IR	Fourier Transform Infrared Spectroscopy
H-K	Horvath-Kawazoe method
HKUST-1	Hong Kong University of Science and Technology-1 metal-organic framework
IUPAC	International Union of Pure and Applied Chemistry
NP's	nanoparticles
SEM-EDS	scanning electron microscopy combined with energy-dispersive X-ray spectroscopy
SE	secondary electron detector
WHO	World Health Organization
XRD	X-ray powder diffraction

REFERENCES

Abenojar J., López de Armentia S., del Real J.C., Martinez M.A., 2024. Magnetic cork as adsorbent to remove hexavalent chromium from aqueous solution. *Appl. Water Sci.*, 14, 267. DOI: 10.1007/S13201-024-02322-Z.

Ahmad W., Qaiser S., Ullah R., Jan B.M., Karakassides M.A., Salmas C.E., Kenanakis G., Ikram R., 2020. Utilization of tires waste-derived magnetic-activated carbon for the removal of hexavalent chromium from wastewater. *Materials*, 14, 34. DOI: 10.3390/MA14010034.

Alagarsamy A.S.K.K., Jiang S.-J., 2017. Synthesis of magnetically separable and recyclable magnetic nanoparticles decorated with β-cyclodextrin functionalized graphene oxide an excellent adsorption of As(V)/(III). *J. Mol. Liq.*, 237, 387–401. DOI: 10.1016/J.MOLLIQ.2017.04.093.

ASTM D4607-14(2021), 2021. *Standard test method for determination of iodine number of activated carbon*. DOI: 10.1520/D4607-14R21.

Azam M., Wabaidur S.M., Khan M.R., Al-Resayes S.I., Islam M.S., 2021. Removal of chromium(III) and cadmium(II) heavy metal ions from aqueous solutions using treated date seeds: an eco-friendly method. *Molecules*, 26, 3718. DOI: 10.3390/MOLECULES26123718.

Bonola B., Sosa-Rodríguez F., Lara R.H., García-Solares S.M., Mena-Cervantes V.Y., Lartundo-Rojas L., Vazquez-Arenas J., Hernández-Altamirano R., 2022. Sustainable and fast elimination of high Cr(III) concentrations from real tannery wastewater using an electrochemical-chemical process forming Cr_2FeO_4. *Sep. Purif. Technol.*, 294, 121211. DOI: 10.1016/J.SEPPUR.2022.121211.

Briffa J., Sinagra E., Blundell R., 2020. Heavy metal pollution in the environment and their toxicological effects on humans. *Heliyon*, 6, e04691. DOI: 10.1016/J.HELIYON.2020.E04691.

Buczek B., Wolak E., 2008. Potassium hydroxide modified active carbon for adsorptive refrigerators. *Adsorption*, 14, 283–287. DOI: 10.1007/s10450-007-9094-5.

Castro-Castro J.D., Sanabria-González N.R., Giraldo-Gómez G.I., 2020. Experimental data of adsorption of Cr(III) from aqueous solution using a bentonite: optimization by response surface methodology. *Data Brief*, 28, 105022. DOI: 10.1016/J.DIB.2019.105022.

Cullity B.D., Graham C.D., 1974. *Introduction to magnetic materials*. 2nd Edition, Wiley-IEEE Press, p. 94.

Dada A.O., Olalekan A.P., Olatunya A.M., Dada O., 2012. Langmuir, Freundlich, Temkin and Dubinin–Radushkevich isotherms studies of equilibrium sorption of Zn^{2+} unto phosphoric acid modified rice husk. *IOSR J. Appl. Chem.*, 3(1), 38–45. DOI: 10.9790/5736-0313845.

Dias D., Lapa N., Bernardo M., Ribeiro W., Matos I., Fonseca I., Pinto F., 2018. Cr(III) removal from synthetic and industrial wastewaters by using co-gasification chars of rice waste streams. *Bioresour. Technol.*, 266, 139–150. DOI: 10.1016/J.BIORTECH.2018.06.054.

Dimas Rivera G.L., Martínez Hernández A., Pérez Cabello A.F., Rivas Barragán E.L., Liñán Montes A., Flores Escamilla G.A., Sandoval Rangel L., Suarez Vazquez S.I., de Haro Del Río D.A., 2021. Removal of chromate anions and immobilization using surfactant-modified zeolites. *J. Water Process Eng.*, 39, 101717. DOI: 10.1016/J.JWPE.2020.101717.

Do M.H., Phan N.H., Nguyen T.D., Pham T.T.S., Nguyen V.K., Vu T.T.T., Nguyen T.K.P., 2011. Activated carbon/Fe_3O_4 nanoparticle composite: fabrication, methyl orange removal and regeneration by hydrogen peroxide. *Chemosphere*, 85, 1269–1276. DOI: 10.1016/J.CHEMOSPHERE.2011.07.023.

Eyvazi B., Jamshidi-Zanjani A., Darban A.K., 2020. Synthesis of nano-magnetic $MnFe_2O_4$ to remove Cr(III) and Cr(VI) from aqueous solution: a comprehensive study. *Environ. Pollut.*, 265, 113685. DOI: 10.1016/J.ENVPOL.2019.113685.

Flieger J., Kawka J., Płaziński W., Panek R., Madej J., 2020. Sorption of heavy metal ions of chromium, manganese, selenium, nickel, cobalt, iron from aqueous acidic solutions in batch and dynamic conditions on natural and synthetic aluminosilicate sorbents. *Materials*, 13, 5271. DOI: 10.3390/MA13225271.

Frolova L., Kharytonov M., 2019. Synthesis of magnetic biochar for efficient removal of Cr(III) cations from the aqueous medium. *Adv. Mater. Sci. Eng.*, 2019, 2187132. DOI: 10.1155/2019/2187132.

Gęca M., Wiśniewska M., Nowicki P., 2022. Biochars and activated carbons as adsorbents of inorganic and organic compounds from multicomponent systems – a review. *Adv. Colloid Interface Sci.*, 305, 102687. DOI: 10.1016/J.CIS.2022.102687.

Guan X., Zhang B., Li D., He M., Han Q., Chang J., 2022. Remediation and resource utilization of chromium(III)-containing tannery effluent based on chitosan-sodium alginate hydrogel. *Carbohydr. Polym.*, 284, 119179. DOI: 10.1016/J.CARBPOL.2022.119179.

Irshad M.A., Sattar S., Nawaz R., Al-Hussain S.A., Rizwan M., Bukhari A., Waseem M., Irfan A., Inam A., Zaki M.E.A., 2023. Enhancing chromium removal and recovery from industrial wastewater using sustainable and efficient nanomaterial: a review. *Ecotoxicol. Environ. Saf.*, 263, 115231. DOI: 10.1016/J.ECOENV.2023.115231.

Krishna Kumar A.S., Warchol J., Matusik J., Tseng W.-L., Rajesh N., Bajda T., 2022. Heavy metal and organic dye removal via a hybrid porous hexagonal boron nitride-based magnetic aerogel. *npj Clean Water*, 5, 24. DOI: 10.1038/S41545-022-00175-0.

Laurent S., Forge D., Port M., Roch A., Robic C., Vander Elst L., Muller R.N., 2010. Magnetic iron oxide nanoparticles: synthesis, stabilization, vectorization, physicochemical characterizations, and biological applications. *Chem. Rev.*, 110, 2574. DOI: 10.1021/CR900197G.

Li R., Chen J., Zhang H., Rehman F., Siddique J., Shahab A., Mo Z., Luo L., 2023. Facile synthesis of magnetic-activated nanocomposites for effective removal of cationic and anionic dyes in an aqueous environment: an equilibrium isotherm, kinetics and thermodynamic studies. *Chem. Eng. Res. Des.*, 189, 319–332. DOI: 10.1016/J.CHERD.2022.11.017.

Liu X., Zhang Y., Liu Y., Zhang T., 2022. Removal of Cr(VI) and Ag(I) by grafted magnetic zeolite/chitosan for water purification: synthesis and adsorption mechanism. *Int. J. Biol. Macromol.*, 222, 2615–2627. DOI: 10.1016/J.IJBIOMAC.2022.10.044.

Maneechakr P., Mongkollertlop S., 2020. Investigation on adsorption behaviors of heavy metal ions (Cd^{2+}, Cr^{3+}, Hg^{2+} and Pb^{2+}) through low-cost/active manganese dioxide-modified magnetic biochar derived from palm kernel cake residue. *J. Environ. Chem. Eng.*, 8, 104467. DOI: 10.1016/J.JECE.2020.104467.

Mao Y., Li Y., Guo Z., Chen B., Qin Z., Zhang Z., Sun J., Gu N., 2022. The coprecipitation formation study of iron oxide nanoparticles with the assist of a gas/liquid mixed phase fluidic reactor. *Colloids Surf., A: Physicochem. Eng. Aspects*, 647, 129107. DOI: 10.1016/J.COLSURFA.2022.129107.

Mawlood I.A., Saod W.M., Al-Rawi A.S., Aljumialy A.M., Hilal N., 2024. Characterization and use of activated carbon synthesized from sunflower seed shell in the removal of Pb(II), Cd(II), and Cr(III) ions from aqueous solution. *Environ. Monit. Assess.*, 196, 364. DOI: 10.1007/s10661-024-12525-1.

Michalak I., Baśladyńska S., Mokrzycki J., Rutkowski P., 2019. Biochar from a freshwater macroalga as a potential biosorbent for wastewater treatment. *Water*, 11, 1390. DOI: 10.3390/W11071390.

Mokrzycki J., Lorenc-Grabowska E., Kordek-Khalil K., Rutkowski P., 2020. Hydrothermal and pyrolytic biochars from waste milk thistle (*Silybum marianum*) extrudates as precursors for production of effective isoproturon adsorbents. *J. Water Process Eng.*, 37, 101459. DOI: 10.1016/J.JWPE.2020.101459.

Mokrzycki J., Michalak I., Rutkowski P., 2021a. Biochars obtained from freshwater biomass – green macroalga and hornwort as Cr(III) ions sorbents. *Biomass Convers. BiorSefin.*, 11, 301–313. DOI: 10.1007/s13399-020-00649-6.

Mokrzycki J., Michalak I., Rutkowski P., 2021b. Tomato green waste biochars as sustainable trivalent chromium sorbents. *Environ. Sci. Pollut. Res.*, 28, 24245–24255. DOI: 10.1007/s11356-019-07373-3.

Mokrzycki J., Wolak E., Orzechowska-Zieba A., Zheng K., Duraczyńska D., Marzec M., Fedyna M., 2024. The effect of copper(II) salt precursor on physicochemical properties of HKUST-1 MOFs and their application as adsorbents of Cr(III) ions from aqueous solutions. *J. Water Process Eng.*, 64, 105761. DOI: 10.1016/J.JWPE.2024.105761.

Nata I.F., Irawan C., Putra M.D., Hudha M.I., Syarkani M.H., Naufal A., 2024. Simultaneous adsorption of Cr(III) ions and contaminants on sugarcane bagasse/rice husk fiber-based amine magnetic biocomposite. *J. Hazard. Mater. Adv.*, 13, 100412. DOI: 10.1016/J.HAZADV.2024.100412.

Ortiz-Quiñonez J.L., Cancino-Gordillo F.E., Pal U., 2023. Removal of Cr(III) ions from water using magnetically separable graphene-oxide-decorated nickel ferrite nanoparticles. *ACS Appl. Nano Mater.*, 6, 18491–18507. DOI: 10.1021/ACSANM.3C03618.

Rouibah K., Ferkous H., Abdessalam-Hassan M., Mossab B.L., Boublia A., Pierlot C., Abdennouri A., Avramova I., Alam M., Benguerba Y., Erto A., 2024. Exploring the efficiency of Algerian kaolinite clay in the adsorption of Cr(III) from aqueous solutions: experimental and computational insights. *Molecules*, 29, 2135. DOI: 10.3390/MOLECULES29092135.

Rusiniak P., Wątor K., Kmiecik E., Vakanjac V.R., 2024. Method validation and geochemical modelling of chromium speciation in natural waters. *Sci. Rep.*, 14, 30502. DOI: 10.1038/s41598-024-77425-3.

Sangkarak S., Kittipongvises S., Kitkaew D., Chaveanghong S., Ittisupornrat S., Phetrak A., Lohwacharin J., 2024. Influence of the iron-oxide mass fractions of magnetic powdered activated carbon on its hexavalent chromium adsorption performance in water. *Chemosphere*, 364, 142997. DOI: 10.1016/J.CHEMOSPHERE.2024.142997.

Shahrokhi-Shahraki R., Benally C., Gamal El-Din M., Park J., 2021. High efficiency removal of heavy metals using tire-derived activated carbon vs commercial activated carbon: insights into the adsorption mechanisms. *Chemosphere*, 264, 128455.S DOI: 10.1016/J.CHEMOSPHERE.2020.128455.

Shehu A., Vasjari M., Duka S., Vallja L., Broli N., 2023. Study of the adsorption efficacy of Cr(III) on a metal oxide-based material derived from the quartz sand enrichment process. *Am. J. Environ. Prot.*, 12, 58–65. DOI: 10.11648/J.AJEP.20231203.11.

Silva V.A.J., Andrade P.L., Silva M.P.C., Bustamante Dominguez A.D., De Los Santos Valladares L., Albino Aguiar J., 2013. Synthesis and characterization of Fe_3O_4 nanoparticles coated with fucan polysaccharides. *J. Magn. Magn. Mater.*, 343, 138–143. DOI: 10.1016/J.JMMM.2013.04.062.

Solis-Ceballos A., Roy R., Golsztajn A., Tavares J.R., Dumont M.J., 2023. Selective adsorption of Cr(III) over Cr(VI) by starch-graft-itaconic acid hydrogels. *J. Hazard. Mater. Adv.*, 10, 100255. DOI: 10.1016/J.HAZADV.2023.100255.

Song X., Liu J., Jiang Q., Zhang P., Shao Y., He W., Feng Y., 2019. Enhanced electron transfer and methane production from low-strength wastewater using a new granular activated carbon modified with nano-Fe_3O_4. *Chem. Eng. J.*, 374, 1344–1352. DOI: 10.1016/J.CEJ.2019.05.216.

Tamjidi S., Esmaeili H., 2019. Chemically modified CaO/Fe_3O_4 nanocomposite by sodium dodecyl sulfate for Cr(III) removal from water. *Chem. Eng. Technol.*, 42, 607–616. DOI: 10.1002/CEAT.201800488.

Thommes M., Kaneko K., Neimark A.V., Olivier J.P., Rodriguez-Reinoso F., Rouquerol J., Sing K.S.W., 2015. Physisorption of gases, with special reference to the evaluation of surface area and pore size distribution (IUPAC Technical Report). *Pure Appl. Chem.*, 87, 1051–1069. DOI: 10.1515/pac-2014-1117.

Wang J., Mao M., Atif S., Chen Y., 2020a. Adsorption behavior and mechanism of aqueous Cr(III) and Cr(III)-EDTA chelates on DTPA-chitosan modified Fe_3O_4@SiO_2. *React. Funct. Polym.*, 156, 104720. DOI: 10.1016/J.REACTFUNCTPOLYM.2020.104720.

Wang S., Nam H., Gebreegziabher T.B., Nam H., 2020b. Adsorption of acetic acid and hydrogen sulfide using NaOH impregnated activated carbon for indoor air purification. *Eng. Rep.*, 2, e12083. DOI: 10.1002/ENG2.12083.

Wijaya R.A., Nakagoe O., Sano H., Tanabe S., Kamada K., 2024. Superior comprehensive performance of modified activated carbon as a hexavalent chromium adsorbent. *Heliyon*, 10, e35557. DOI: 10.1016/j.heliyon.2024.e35557.

Wilson K., Iqbal J., Obaid Abdalla Obaid Hableel A., Naji Khalaf Beyaha Alzaabi Z., Nazzal Y., 2024. Camel dung-derived biochar for the removal of copper(II) and chromium(III) ions from aqueous solutions: adsorption and kinetics studies. *ACS Omega*, 9, 11500–11509. DOI: 10.1021/ACSOMEGA.3C08230.

Wu Z., Zhang H., Ali E., Shahab A., Huang H., Ullah H., Zeng H., 2023. Synthesis of novel magnetic activated carbon for effective Cr(VI) removal via synergistic adsorption and chemical reduction. *Environ. Technol. Innovation*, 30, 103092. DOI: 10.1016/J.ETI.2023.103092.

Xu T., Gan D., Wei G., Yang Y., Wei Q., He C., 2025. Adsorption of Cr(III) by IRA-900 resin in sodium phosphite and sulfuric acid system. *Separations*, 12, 270. DOI: 10.3390/SEPARATIONS12100270.

Yang S., Li L., Pei Z., Li C., Lv J., Xie J., Wen B., Zhang S., 2014. Adsorption kinetics, isotherms and thermodynamics of Cr(III) on graphene oxide. *Colloids Surf., A: Physicochem. Eng. Aspects*, 457, 100–106. DOI: 10.1016/J.COLSURFA.2014.05.062.

Yuan B., Yang Z., Wu P., Yin X., Liu C., Sun F., He J., Jiang W., 2025. Efficient treatment of chromium-containing wastewater based on auxiliary intelligent model with rapid-response adsorbents. *Sep. Purif. Technol.*, 363, 132037. DOI: 10.1016/J.SEPPUR.2025.132037.

Zhang Y.-N., Yu Y.-X., 2018. Adsorptive removal of Cr^{3+}, Cu^{2+}, and Ni^{2+} ions by magnetic Fe_3O_4@alkali-treated coal fly ash. *Desalin. Water Treat.*, 123, 277–287. DOI: 10.5004/DWT.2018.22778.